Magnesium Technology 2011
Edited by: Wim H. Sillekens, Sean R. Agnew, Neale R. Neelameggham, and Suveen N. Mathaudhu
TMS (The Minerals, Metals & Materials Society), 2011

DEFORMATION BEHAVIOR OF FRICTION STIR PROCESSED MAGNESIUM ALLOYS

Q. Yang[1], S. Mironov[2], Y.S. Sato[2], K. Okamoto[3]
[1]Research and Development Division, Hitachi America, Ltd., Farmington Hills, MI 48335, USA
[2]Department of Materials Processing, Tohoku University, Sendai 980-8579, JAPAN
[3]Hitachi Research Laboratory, Hitachi Ltd., Ibaraki 319-1292, JAPAN

Keywords: Mg alloy, Friction stir processing, Anisotropy of mechanical properties, texture

Abstract

The present study explores the feasibility of using friction stir processing to produce high-performance Mg alloy sheet. Deformation behavior of friction stir processed Mg alloys is addressed. Analyses of grain size and crystallographic texture are made to interpret the characteristics of strength and ductility of friction stir processed Mg. It is found that friction stir processing causes variation of texture orientation in the processed sheet. The non-uniform texture distribution leads to significant in-plane anisotropy in ductility as well as localized deformation behavior of the processed sheet. Furthermore, the inhomogeneity of high-intensity texture would not be eliminated by hot compression performed along the normal of the processed sheet.

Introduction

Wrought Mg alloys in the forms of sheet and extrusion have been extensively investigated with a target for lightweight structural applications [1,2]. Ultra-fine grained (UFG) Mg alloys produced through severe plastic deformation processing exhibit excellent attributes such as higher yield/tensile strength and formability as well as less strength anisotropy, compared to coarse grained material [3-5]. In this study, the feasibility of using friction stir processing (FSP) to produce high-performance Mg alloy sheet is explored.

FSP, derived from friction stir welding (FSW), is enforced by a non-consumable tool which consists of a circular shoulder and a profiled pin [6]. The tool pin is fully penetrated in the bulk material with the shoulder in contact with the upper plate surface while the rotating tool is translated. Frictional heat and large-strain shear deformation mainly resulted from the rotation of the tool pin enable the processed material to flow around the tool and finally deposit at the back of the tool. The tool is shifted in the transverse direction by a certain distance after each single pass such that there is an overlap between the neighboring beads, as schematically illustrated in Fig. 1(a). Repeat the process until the base material is entirely processed. The heavily deformed material undergoes dynamic recrystallization during process and subsequent static recrystallization, and would be transformed into uniform ultra-fine grained material. FSP has been applied to refining grain structure in various Al alloys and hence developing superplastic forming [7,8].

Mg alloy has a hexagonal close-packed (HCP) crystal structure, and mechanical properties of wrought Mg exhibit high texture-dependence. The present study addresses the characteristics of strength and ductility of friction stir processed (FSPed) Mg alloy. Analyses of grain size and texture are first conducted on a single-pass processed bead, and the deformability of a fully processed Mg is then briefly discussed.

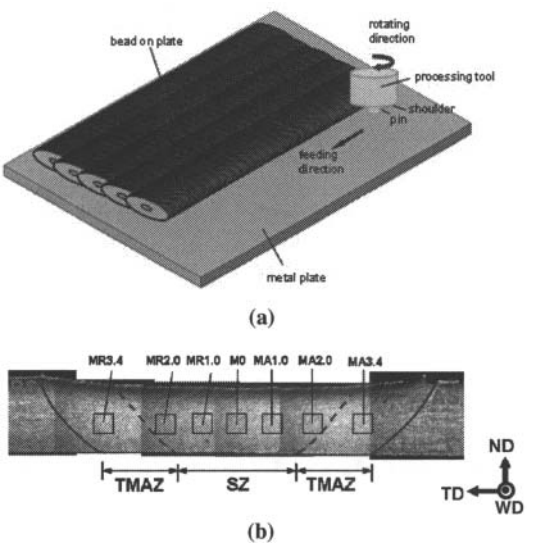

Fig. 1 (a) Illustration of FSP; (b) Cross sectional macrostructure of a single-pass processed bead

Experiment

Hot rolled AZ31 Mg alloy sheet 2.0mm thick was chosen for the present study. The processing tool consisted of a 10mm-diameter shoulder and a 4mm-diameter threaded pin which was 1.75mm long. FSP was conducted at selected rotational speeds of 1500, 2000 and 3000rpm and a selected travel speeds of 100 mm/min. The tool translation direction (WD) was perpendicular to the sheet rolling direction (RD).

Microstructural examination was made on a plane containing the sheet normal direction (ND) and RD for the base alloy, and on a plane containing the ND and transverse direction (TD) for FSPed beads. The TD is perpendicular to the WD. All specimens were subjected to mechanical grinding and polishing. The specimens are etched with an acetic-picral solution. Orientation image microscopy (OIM) was conducted for texture analysis, with each individual scanning area being 600μm x 600μm.

Mechanical properties of the base metal and the FSPed beads along the WD and TD were investigated by uni-axial tension. Test specimens with gauge width and length of 4 and 20 mm, 6 and 30 mm, and 10 and 55 mm were cut from FSPed beads along the WD with the longitudinal centerlines of tensile specimens and processed beads coincident, as exemplified in Fig. 2. Test specimens cut from the base metal along the RD and from the

FSPed beads along the TD had 6mm gauge width and 30mm gauge length. Sectioned specimens from the processed beads were subject to grinding from the top processing surface and the bottom surface by about 0.2mm deep prior to testing. Specimens were tested at an initial strain rate of $8.33\times10^{-4}s^{-1}$.

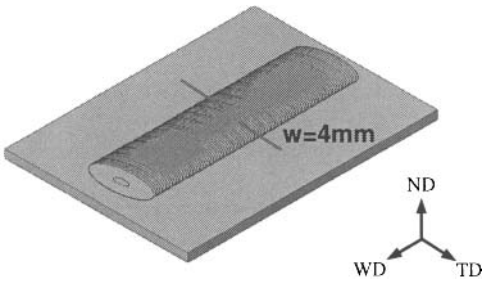

Fig. 2. Illustration of specimen sectioning from a FSP bead along the WD

Results

Microstructure and mechanical property of single-pass FSPed beads

A single bead has an advancing side (AS) and a retreating side (RS) that are located on the two sides of the tool. On the AS, the shear stress induced by the pin rotation has a similar direction to that induced by the forward tool pin translation, while on the RS, the directions of these two shear stresses are opposite. Fig. 1(b) shows macrostructure of a processed bead. Macroscopically, an individual bead can be partitioned into a central stir zone (SZ) and two thermo-mechanical zones (TMAZ) that are covered by the SZ's of the prior and subsequent beads during FSP.

Fig. 3 shows microstructure variation in a bead which is made at 3000rpm. In the center of the bead, a bimodal grain structure is present near the top surface (Fig. 3(a)). The microstructure then becomes quite uniform but coarser through the mid-layer (Fig. 3(d)) towards the bottom surface (Fig. 3(g)). In the mid-layer (Fig. 3(b-f)), microstructure uniformity increases from the TMAZ to the SZ center. Large and elongated grains are present in the TMAZ's. The locations of the mid-layer microstructures are indicated on the micrographs. For example, MR3.4 and MA3.4 represent the locations 3.4mm from the bead center on the RS and AS, respectively.

Fig. 4(b-d) shows the effect of rotation speed on microstructure in the SZ center. The microstructure of the base metal is also included for comparison (Fig. 4(a)). The base metal has a bimodal grain structure with an average grain size of 7.9μm. Grain size and uniformity of FSPed material are affected by process condition. As shown, grain size increases with rotation speed. The average grain sizes in the SZ's are 2.6μm, 7.6μm and 12.0μm at 1500, 2000 and 3000rpm, respectively. The SZ shows a banded structure composed of fine and coarse grain band at 1500rpm, while it shows a nearly uniform microstructure at a rotation speed of 3000rpm.

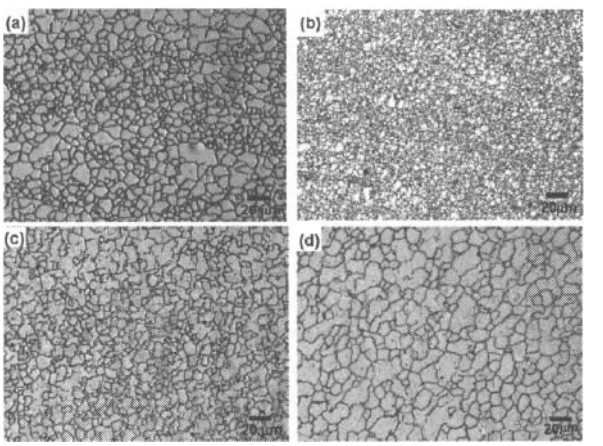

Fig. 4 (a) Microstructure of the base metal; (b-d) Microstructures of the SZ at 1500, 2000, and 3000rpm, respectively.

The rolled base metal has a texture in which the (0002) basal poles are aligned with the ND. FSP develops very strong shear texture in the weld region. Texture mapping along the thickness in the bead center shows: (1) the top surface region about 0.3mm deep has a basal texture tending to be aligned with the surface (*i.e.*, nearly [0002]//ND). This indicates that the tool shoulder dominates plastic deformation in this region; (2) the rotation of the tool pin dominates plastic deformation inside the metal sheet, leading to a single basal fiber in which the (0002) basal poles are roughly aligned with the WD (*i.e.*, the basal planes are parallel to the pin surface). Therefore, texture in the mid-layer across the bead is only shown here. The measurement locations as indicated are consistent with those marked in Fig. 1(b).

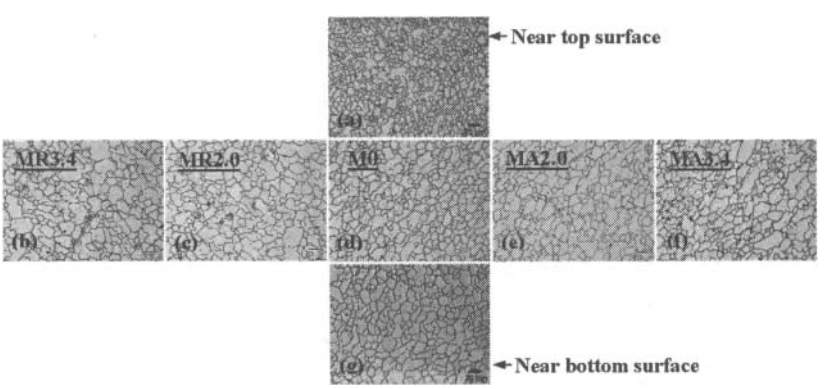

Fig. 3. Microstructures of a single bead made at 3000rpm and 100mm/min.

As shown in Fig. 5, the location 'M0' is the bead center which has a single basal fiber texture (*i.e.*, nearly [0002]//WD). The intensity of basal texture is expressed as times random. On the RS, the location 'MR2.0' is the stir zone extremity where the basal texture splits into two components of similar intensities. In one component, the basal planes are approximately parallel to the pin surface but have a rotation around the plate normal direction (ND). In the other component, the basal planes show a further rotation around the WD from the orientation of the former component. The location 'MR3.4' is immediately close to the base material, and shows a dominant texture component close to the texture of the base metal. Therefore, from the base material to the bead center on the RS, the basal planes aligned with the sheet surface, experiences two rotations around the WD and ND in sequence, to reach the orientation aligned with the pin surface. On the AS, the texture undergoes similar evolution from the base material towards the weld center. It is worth noting that in the location 'MA2.0', the texture splits into two components as well. The component where the basal planes are tilted from the ND by about 40° might be induced by the upward flow of the plasticized material due to the tool translation while this material is dragged into the rotational shear zone around the tool pin due to the tool rotation. The material is subsequently aligned with the pin surface due to the shearing effect, as indicated by nearly (0002) // the pin surface (*i.e.*, the other component).

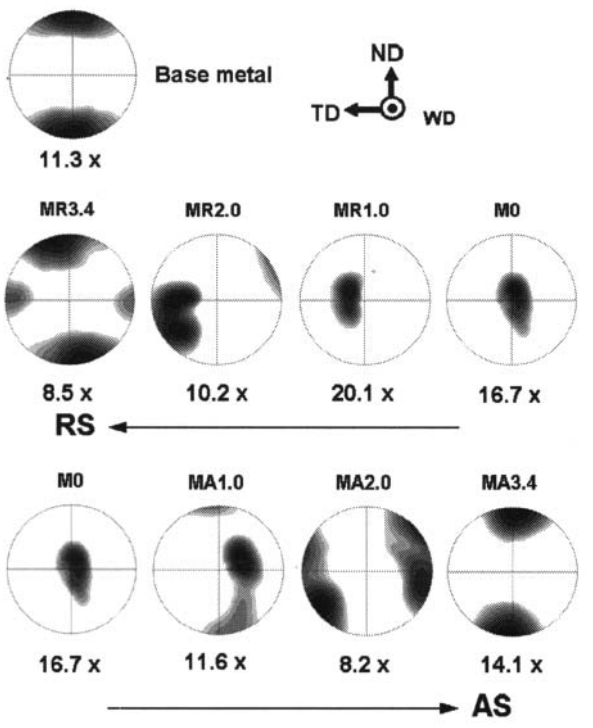

Fig. 5. {0002} pole figures of as received and FSPed AZ31 Mg alloy.

A lower rotation speed of 1500rpm results in cavity in the SZ of the bead near the bottom surface, and mechanical properties at this process condition are therefore not evaluated. Fig. 6(a) shows mechanical properties of defect-free beads along the TD. The base metal has yield strength of 171MPa, ultimate tensile strength of 265MPa, and elongation of 20.1%. The processed beads have yield strengths of about 75MPa and elongations of 3.5%-4.7%; the tensile strength is increased from 196MPa to 225MPa when the rotation speed is raised from 2000rpm to 3000rpm.

Fig. 6(b) indirectly examines the variation with the location of mechanical properties of the processed material in a bead along the longitudinal direction (LD, same as WD). Take the bead made at 3000rpm for example. Since the processed region in a bead is in the shape of a basin, the test specimen 10mm wide includes undisturbed material which is positioned out of the TMAZ's. As shown, increasing specimen width increases yield strength but decreases ductility; it does not result in a prominent increase in ultimate tensile strength. Corresponding to the specimen widths of 4, 6 and 10mm, the yield strengths are 62, 67 and 114MPa, respectively; the tensile strengths are 225, 225 and 243MPa, respectively. The ductility decreases from 36.5% to 26.8% to 20%.

Fig. 6(c) shows the effect of rotation speed on mechanical properties of processed bead along the LD. Test specimen has a gauge width of 4mm. Increasing rotation speed (and therefore grain size) slightly increases both yield strength (from 52Mpa to 62MPa) and tensile strength (from 195MPa to 225MPa), but decreases ductility from 47% to 36.5%.

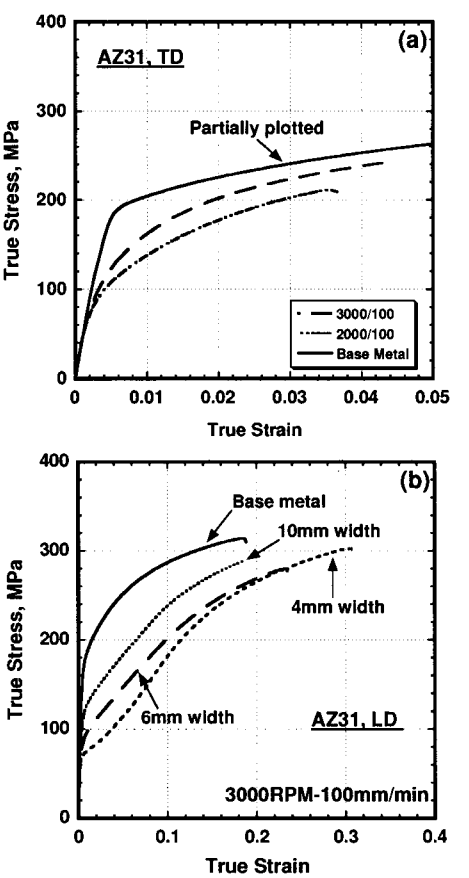

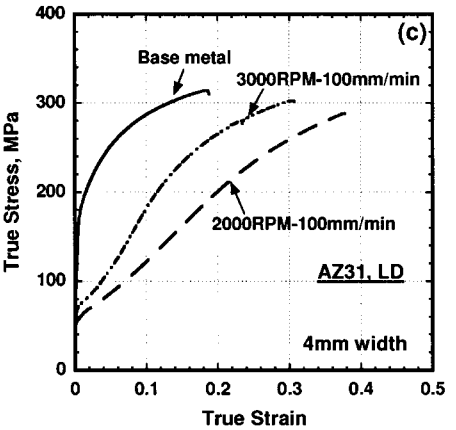

Fig. 6. Mechanical properties of single-pass FSPed beads along the TD and LD

Deformability of multiple-pass FSPed Mg

Fig. 7(a) shows the geometry of a failed tensile specimen. The specimen is cut along the TD from a single-pass AZ31 Mg bead which is made at 3000rpm. As shown, the specimen fails ~2mm from the bead center on the AS after increased local deformation over there (distance measured from the mid-layer). Significant necking is also found at the corresponding location on the RS. Further examination of the geometrical change of the circular grid pattern marked on the tensile specimen shows that the material in the center of the bead is hardly deformed, and that the material near the regions of deformation localization and the fracture surface undergoes appreciable deformation and rotation.

Fig. 7(b) shows the geometry of a failed tensile specimen which is cut from a fully FSPed AZ61 Mg along the TD. The AZ61 Mg alloy is first friction stir processed and then compressed at 300°C with more than 50% thickness reduction. Mechanical testing shows that the step of hot compression increases the ductility of the FSPed material along the TD. However deformation localization still remains. Figs. 6 and 7 indicate that FSP develops strong in-plane anisotropy in deformability of Mg alloys. In other words, FSP enhances the ductility of Mg alloy along the tool travel direction (WD). However it deteriorates the ductility in the perpendicular direction (TD) by developing deformation localization.

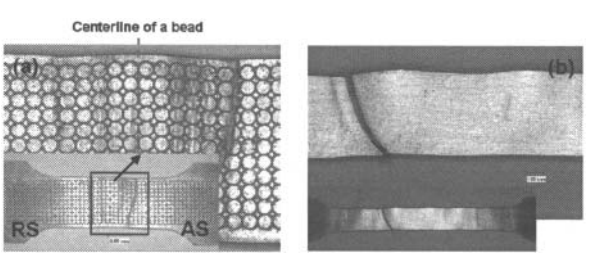

Fig. 7. Geometry of failed tensile specimens showing the formability along the TD of: (a) a single-pass FSPed AZ31; (b) a multiple-pass FSPed AZ61.

Discussion

Friction stir processing, like other severe plastic deformation processes such as ECAE and high pressure torsion, develops a strong ***B***-fiber texture in Mg alloys where the basal plane (0002) is aligned with the substantive shear plane [9-11]. For FSP, the shear plane is mainly the tool pin surface, and therefore leading to (0002)//ND nearly in the SZ (Fig. 5). Across the TMAZ's, the basal plane undergoes two rotations, first around the WD and then around the ND, to achieve the reorientation of crystallographic texture from the base material to the processed SZ. The texture evolution discloses material flow driven by the tool on the two sides of the processing tool.

Mg alloys have a limited number of slip systems at low temperatures due to their HCP crystal structure. The potential mechanisms for deforming Mg at such temperatures mainly include the basal <a>, the prismatic <a>, and the tensile $\{10\bar{1}2\}$ twinning [12-14]. Each individual deformation mode has its own critical resolved shear stress (τ_{CRSS}). With a designated texture orientation with respect to the external loading direction, each deformation mode corresponds to a yield stress σ_y according to the Schmid's law

$$\sigma_y = \tau_{CRSS} / m \quad (1)$$

, where m is an average Schmid factor for such a deformation mode. The deformation mode having the smallest yield stress is activated.

The single-pass FSPed material exhibits texture orientations in which the (0002) basal planes are considerably tilted from the sheet plane (Fig. 5). In addition, the basal <a> slip system has a τ_{CRSS} significantly lower than those for the other two deformation modes. Therefore, the basal **<a>** slip would expectably dominate plastic flow at the early stage of deformation.

Consider the effect of distributed texture on deformation behavior of single-pass FSPed material. Calculation shows that the locations 'MA2.0' and 'MR2.0' have the largest m values for the basal **<a>** slip when a bead is loaded along the TD. From Eq. (1), plastic deformation in a Mg bead is initiated from these two locations. The basal poles tilted in the tensile direction (*i.e.*, the TD) enhances the occurrence of mechanical twinning and disfavors the activation of the prismatic slip [2,12,15]. A preliminary microstructure analysis of the failed TD specimens also indicates that the regions 'MA2.0' and 'MR2.0' are severely twinned, and the central area 'M0' and other regions are much less deformed. In Mg, mechanical twins are barriers to dislocation motion, and the induced stress concentration is generally unlikely to be relaxed by other slips, kinking or twinning at an ambient temperature. Therefore, the localized deformation accelerates the failure of the FSPed material with a relatively low strength (Fig. 6(a)).

When the loading direction is along the WD, the m values for the basal **<a>** slip are the largest in the locations 'MA1.0' and 'MR1.0', leading to lower yield strength of the processed material compared to the base metal (Fig. 6(b) and (c)). The extensive twinning takes place in the processed material as well. These two factors result in an increase in strain hardening rate which is the essential reason for ductility enhancement. The rate-sensitivity of the processed material is significantly lower than that of the base

material. The present study shows that the grain size effect is not as important as the texture effect on mechanical properties of Mg when different grain sizes are in a comparable range.

Tensile testing of a FSPed and hot pressed Mg alloy along the TD shows evenly-spaced deformation localization (Fig. 7(b)). This indicates that the variation of text orientation caused by FSP would not be eliminated by hot compression. The texture evolution in the FSPed material during hot compression is under investigation to better understand its effect on the deformation behavior of 'modified' FSPed material. The present study shows that eliminating the variation of texture orientation is the key to enabling FSP to produce high-performance wrought Mg sheet.

Conclusions

(1) Friction stir processing results in significant reduction of yield strength and ultimate tensile strength, and develops strong anisotropy of ductility in Mg alloy. The reorientation of crystallographic texture by friction stir processing dominates these changes of mechanical properties.
(2) The variation of texture orientation caused by FSP would not be eliminated by hot pressing.
(3) Eliminating the variation of texture orientation is the key to enabling friction stir processing to produce high-performance wrought Mg sheet.

References

[1] J. Bohlen, J. Swiostek, D. Letzig, K.U. Kainer, Magnesium technology 2009 (2009), 225-230.
[2] J. Bohlen, M.R. Nurnberg, J. Senn, D. Letzig, S.R. Agnew, Acta Materialia 55 (2007) 2101-2112.
[3] Q. Yang, A.K. Ghosh, Acta Materialia 54 (2006) 5147-5158.
[4] Q. Yang, A.K. Ghosh, Acta Materialia 54 (2006) 5159-5170.
[5] Q. Yang, A.K. Ghosh, Metall. Mater. Trans. A 39A (2008) 2781-2796.
[6] W.M. Thomas, E.D. Nicholas, J.C. Needham, M.G. Murch, P. Templesmith, C.J. Dawes, G.B. Patent Application No. 9125978.8, Dec. 1991.
[7] Z.Y. Ma, R.S. Mishra, M.W. Mahoney, Acta Materialia, 50 (2002) 4419-4430.
[8] Z.Y. Ma, R.S. Mishra, M.W. Mahoney, R. Grimes, Metall. Mater. Trans. A 36A (2005) 1447-1458.
[9] Y.S. Sato, H. Kokawa, K. Ikeda, M. Enomoto, S. Jogan, T. Hashimoto, Metall. Mater. Trans. A 32A (2001) 941-948.
[10] S.H.C. Park, Y.S. Sato, H. Kokawa, Metall. Mater. Trans. A 34A (2003) 987-994.
[11] B Beausir, L.S. Toth, K.W. Neale, Acta Mater 55 (2007) 2695.
[12] D.L. Yin, J.T. Wang, J.Q. Liu, X. Zhao, Magnesium technology 2009 (2009), 235-240.
[13] A. Staroselsky, L. Anand, International Journal of plasticity 19 (2003) 1843-1864.
[14] S.R. Agnew, C.N. Tome, D.W. Brown, Scripta Materialia 48 (2003) 1003-1008.
[15] X. Huang, K. Suzuki, A. Watazu, I. Shigematsu, N. Saito, Mater. Sci. Eng. A 488 (2008) 214-220.